Published in final edited form as:
Biochemistry. 2012 January 10; 51(1): 214–224. doi:10.1021/bi201707v.

Post–translational Modifications of Serotonin Type 4 Receptor Heterologously Expressed in Mouse Rod Cells†

David Salom[⊥,‡], **Benlian Wang**[⊥,§], **Zhiqian Dong**[‡], **Wenyu Sun**[‡], **Pius Padayatti**[‡], **Steven Jordan**[#], **John A. Salon**[#], and **Krzysztof Palczewski**[¤,‡,*]

[‡]Polgenix Inc., Cleveland, Ohio 44106, USA

[¤]Department of Pharmacology, School of Medicine, Case Western Reserve University, Cleveland, Ohio 44106, USA

[§]Center for Proteomics and Bioinformatics, School of Medicine, Case Western Reserve University, Cleveland, Ohio 44106, USA

[#]Department of Molecular Structure, Amgen Incorporated, Thousand Oaks, CA 91320–1799, USA

Abstract

The G–protein–coupled serotonin receptor type 4 (5–HT_4R) is a pharmacological target implicated in a variety of gastro-intestinal and nervous system disorders. Like many other integral membrane proteins, structural and functional studies of this receptor could be facilitated by its heterologous overexpression in eukaryotic systems that can perform appropriate post–translational modifications (PTMs) on the protein. We previously reported the development of an expression system that employs rhodopsin's biosynthetic machinery in rod cells of the retina to express heterologous G–protein coupled receptors (GPCRs) in a pharmacologically functional form. In this study, we analyzed the glycosylation, phosphorylation, and palmitoylation of 5–HT_4R heterologously expressed in rod cells of transgenic mice. We found that the glycosylation pattern in 5–HT_4R was more complex than in murine and bovine rhodopsin. Moreover, overexpression of this exogenous GPCR in rod cells also affected the glycosylation pattern of coexisting native rhodopsin. These results highlight not only the occurrence of heterogeneous PTMs on transgenic (TG) proteins, but also the complications that non–native PTMs can cause in the structural and functional characterization of both endogenous and heterologous protein targets.

G–protein–coupled receptors (GPCRs) are versatile biological sensors. They are pivotal regulators of cellular responses to a wide spectrum of hormones and neurotransmitters, and are involved in a broad range of sensory physiology including sight, smell and taste (1). In mammals, the 5–hydroxytryptamine (5–HT, serotonin) family of receptors (5–HTRs) have been implicated in a variety neurological and systemic functions including modulation of memory, aggression, appetite, sexuality, sleep, cognition, thermoregulation, perception, reward, anger and mood (2, 3). 5–HT_4Rs also could serve as targets for the development of new drugs to treat Alzheimer's disease, congestive heart failure, opioid-induced respiratory

†This research was supported, in part, by National Institutes of Health Grants EY009339 and P30 EY019478. KP is John H. Hord Professor of Pharmacology.

*To whom correspondence should be addressed: Krzysztof Palczewski, Ph.D. Phone: (216) 368–4631. Fax: (216) 368–1300. kxp65@case.edu.
⊥These authors contributed equally to this work.

SUPPORTING INFORMATION AVAILABLE Supporting information contains a SEC profile, mass spectroscopy coverage and mass spectra for purified 5-HT_4R from TG mice, and SDS-PAGE gels and immunoblots for several GPCRs. This material is available free of charge via the Internet at http://pubs.acs.org.

depression, feeding-associated diseases such as anorexia and major depressive disorders, and is the target of drugs to treat gastrointestinal diseases such as chronic idiopathic constipation (3, 4).

Most GPCRs are naturally expressed at such low levels, rhodopsin constituting a notable exception, that heterologous expression systems must be used to obtain sufficient material for their biophysical characterization. *In vitro* eukaryotic cell systems are most often employed for this purpose because they can perform the complex post–translational modifications (PTMs) required for efficient membrane targeting, stability and function.

With improved detection technologies, the list of protein modifications reported has risen to over 300 (5, 6). Some PTMs, such as phosphorylation, are transient even though they play essential roles in intracellular signaling. Others, including glycosylation, lipidation and disulfide bridge formation, are more stable and these are important for maturation and proper folding of newly synthesized proteins (7). N-Glycosylation is one of the most common forms of post-translational modification, and it is intricately involved in various cellular processes including protein folding, protein secretion, intracellular trafficking, stability, binding affinity, enzyme activity, and substrate specificity, enabling the fine-tuning of a protein's function (8).

Heterogeneity of its PTMs can interfere with the function, stability and/or crystallizability of a recombinant protein. Homogeneity of a protein population used for crystallization campaigns is usually judged by the sharpness of its electrophoretic band, heterogeneous glycosylation being the main cause of band smearing. For this reason, proteins destined for crystallization trials are often enzymatically or mutationally deglycosylated. Size–exclusion chromatography (SEC) is used routinely to judge sample oligomerization/polydispersity, but the resolution of SEC is generally not sufficient to separate different post-translationally modified protein species (with the possible exception of hyperglycosylated proteins). In addition, many other PTMs causing population heterogeneity that can be potentially detrimental for expression, functional characterization or crystal growth, are not evident on SDS–PAGE gels. In these cases more laborious techniques or strategies are needed to detect and eliminate population heterogeneity (6).

Our laboratory has developed an *in vivo* system for the expression of GPCRs in rod photoreceptors of *Xenopus* (9) and mice (10, 11). This system was validated with tens of different GPCRs, co–expressed as a transgene along with rhodopsin in retinal rod cells. Characterization of four of these recombinant GPCRs (adenosine A1 receptor ($A_{A1}R$), 5-HT_4R, 5-HT_1AR and sphingosine-1-phosphate receptor 1) revealed that they were produced in a pharmacologically relevant conformation and that their glycosylation pattern was more homogeneous than when they were expressed in mammalian cell culture.

In this work we further examined the PTMs of 5–HT_4R expressed in mouse rod cells with the aim of minimizing protein heterogeneity prior to embarking upon crystallization trials. Our analysis indicated that PTMs of 5–HT_4R were heterogeneous when expressed in this system. We also analyzed murine rhodopsin for comparison and found that its glycosylation pattern was more heterogeneous in the presence of co-expressed 5-HT_4R. These results shed light on the biosynthesis and processing of GPCRs both in rod cells specifically, and in other heterologous expression systems in general, and highlight the often unaddressed occurrence of such non–native PTMs in recombinant proteins.

EXPERIMENTAL PROCEDURES

Transgenic mice

Generation of 5–HT_4R TG mice was described in detail previously (10, 11). In brief, the recombinant vector used to generate this TG mouse line contained the mouse rhodopsin promoter, followed by the full–length coding sequence for human 5–HT_{4b}R and the immunopurification tags T7 (MASMTGGQQMG) and Rho15 (C–terminus of rhodopsin). The recombinant expression construct was microinjected into 18–h–old hybrid C57BL/6J and FVB/NJ embryos (Taconic, Germantown, NY) which were then implanted into pseudo-pregnant female mice to produce the founder stock. To minimize random insertion of the artificial transgene, interference with other gene(s) or vice versa, we first selected founders based on the highest expression level of the transgene by their offspring. Then we determined by gel electrophoresis and immunohistochemistry that 3-week-old mice exhibited the highest expression levels of 5-HT_4R.

Purification of 5–HT_4R and rhodopsin

For the purification of 5–HT_4R, eyes were enucleated from 3–week–old offspring of TG and WT mice and then frozen. Typically 4,000–6,000 frozen eyes were ground to a fine powder with a mortar and pestle under liquid nitrogen. All the subsequent steps were performed at 4°C. The frozen powder was transferred to a Dounce tissue grinder, and homogenized further in 20 mM Tris buffer, pH 7.4 (with protease inhibitors, 10 μg/ml benzamidine and 1 mM phenylmethanesulfonyl fluoride). The 5-HT_4R antagonist, GR125487, was kept at 250 nM at all times during the purification, except during receptor centrifugal concentration when the concentration was increased to avoid ligand depletion. The suspension was centrifuged for 30 min at 48,400*g* at 4°C and the supernatant was discarded. The membrane pellet was resuspended in 1 L of TBS (50 mM Tris, pH 7.4, 280 mM NaCl, 6 mM KCl) and solubilized with 0.1% (w/v) *n*–dodecyl–β–D–maltoside (DDM) and 0.1% (w/v) 3–[(3–cholamidopropyl)dimethylammonio]–1–propanesulfonate (CHAPS) with rotation for 3–4 hours. Insoluble material was removed by centrifugation (45 min, 8,700*g*) and paper filtration. The supernatant was incubated with slow rotation overnight with 13 mL of agarose–immobilized T7 antibody (Novagen, Madison, WI) and then loaded onto a column. The T7 column was washed with 200 mL of washing buffer (1 mM DDM in TBS), and eluted overnight with 200 mL of T7 competing peptide (MASMTGGQQMG) in washing buffer. Immediately before this elution, a 3.5–mL column with agarose–immobilized 1D4 monoclonal antibody (12) was coupled in tandem to the T7 column to capture the eluted receptor. After elution, the T7 column was removed, and the 1D4 resin was washed and eluted with 1D4 competing peptide (TETSQVAPA) in washing buffer. The eluate was concentrated to 1 mL, and loaded in two runs onto a SEC Superdex 200 column (GE healthcare, Piscataway, NJ) equilibrated with washing buffer. The resulting fractions containing 5–HT_4R were concentrated with 50 kDa centrifugal concentrators to 1–2 mg/mL and separated in NuPAGE 4–12% polyacrylamide SDS–PAGE gels (Invitrogen, Carlsbad, CA). Receptor bands were cut out from gels after staining with Coomassie G–250 (SimplyBlue SafeStain, Invitrogen) and used for mass spectrometry (MS) analyses. The typical yield for a preparation of this scale was about 1 mg of purified 5–HT_4R.

WT mouse rhodopsin from TG mice expressing 5–HT_4R was purified from the flow–through of the T7 column after the first step of 5–HT_4R purification. (This contained just trace amounts of 5–HT_4R but all the mouse rhodopsin). Rhodopsin was purified with a 1D4 column and Superdex 200 column in a manner similar to 5–HT_4R.

Rhodopsin from WT mice was purified from twenty-two WT mouse eyes. Eyes were homogenized in a glass Dounce tissue grinder and the sample was treated in a manner

similar to 5–HT_4R, except that the T7 purification step was omitted. Bovine rhodopsin was purified from retinas in a manner similar to mouse rhodopsin except that rod outer segments (ROS) were isolated from dark adapted bovine retinas (13) before detergent solubilization (14).

For polysaccharide analyses, ~10% of a purified sample (5–HT_4R or rhodopsin) was incubated with PNGase F prior to SEC, and the resulting preparation was used as a deglycosylated control. For phosphorylation analyses, all 5–HT_4R samples were deglycosylated. To obtain the corresponding dephosphorylated control sample, ~10% of the purified 5–HT_4R was treated with mouse protein phosphatase PP2A (15).

Mass Spectrometry

Bands from SDS–PAGE gels containing 5–HT_4R were subjected to in-gel digestion with either sequencing grade modified trypsin (Promega, Madison, WI) or chymotrypsin (Roche, Indianapolis, IN) according to the procedure described previously (16). Briefly, pieces excised from a SDS–PAGE gel were first de-stained in 50% acetonitrile containing 50 mM ammonium bicarbonate and then dehydrated with acetonitrile. Before an overnight proteolytic digestion, proteins were reduced with 20 mM DTT at room temperature for 1 h and alkylated with 50 mM iodoacetamide in 50 mM ammonium bicarbonate for 30 min in the dark. After proteolytic digestion, peptides were extracted from the gel with 5% formic acid in 50% acetonitrile and then resuspended in 0.1% formic acid after being dried completely under vacuum. Identification of 5–HT_4R phosphorylaytion sites was facilitated by removal of sugar chains from the protein with PNGase F, as well as by enrichment of phosphopeptides with a MonoTip TiO column (GL Science Inc, Tokyo, Japan) according to the manufacturer's protocol. Liquid chromatography–tandem mass spectrometry (LC-MS/MS) analysis of the resulting peptides was performed with a LTQ Orbitrap XL linear ion trap mass spectrometer (Thermo Fisher Scientific, Waltham, MA). Reverse–phase HPLC was carried out with an Ultimate 3000 HPLC system (Dionex, Sunnyvale, CA) equipped with a Dionex C18 Acclaim PepMap 100 column (0.075 mm × 150 mm). Mass spectra were acquired by using alternating full and MS/MS scans of the five most abundant precursor ions at the normalized collision energy of 30%. Mass spectrometric data were analyzed with Mascot Daemon (Version 2.3.0, Matrix Science, London, UK). Phosphorylation of Ser, Thr and Tyr residues, palmitoylation of Cys, carbamidomethylation of Cys residues (due to the iodoacetamide treatment), as well as oxidation of Met residues were set as variable modifications. Phosphorylation sites suggested by the MASCOT search were verified by manually examining each tandem mass spectrum of phosphopeptides. For the glycosylation study, candidate N–glycosylated sites were initially identified with glycan–free peptides based on the conversion of Asn residues to Asp by PNGase F. Sugar compositions of glycopeptides were verified by manual interpretation of the obtained tandem mass spectra.

For glycosylation analyses, murine and bovine rhodopsins were treated similarly to 5–HT_4R.

RESULTS

Different heterologous expression systems have been shown to introduce varying PTMs in the same protein. For example rhodopsin is heavily and heterogeneously glycosylated when expressed in HEK293 and COS–1 cells (17), yeast (18), NIH 3T3 cells (*this work*) and mouse liver (11), in contrast to more sparse and homogeneous glycosylation pattern seen in its native retinal tissue (19).

To investigate this phenomenon, we carried out a detailed comparative analysis of PTMs present in recombinant 5–HT_4R expressed in rod cells versus 5–HT_4R expressed in other systems, and included rhodopsin as a reference GPCR. Based on amino acid sequence,

PTMs predicted for 5–HT_4R were S–palmitoylation at C^{328} and *N*–linked glycosylation at N^7 and N^{180} (20). A disulfide bridge between C^{93}–C^{184} was also predicted based on homology to other GPCRs (21) and experimental data (22). Residues T^{218}, T^{248} and S^{318} are potential protein kinase C phosphorylation sites and its C-terminus is rich in serine and threonine residues, some of which are potential phosphorylation sites for G protein-coupled receptor protein kinases (23) (20).

N–glycosylation of 5–HT_4R

There are two putative *N*–linked glycosylation sites in the extracellular side of 5-HT_4R that conform to the consensus sequence N–X–S/T, where X can be any amino acid except a Pro residue. These are located on the extracellular side of 5–HT_4R (N^7 in the N–terminus and N^{180} in the extracellular loop E–II) (Figure 1). Initial electrophoresis in 12% polyacrylamide gels showed a single band for 5–HT_4R expressed in rod cells of TG mice (10), and SEC on Superdex 200 revealed a sharp, single major peak (Figure S1). Further analysis in 4–12% acrylamide NuPAGE gradient gels (Invitrogen) revealed a minor band with slightly higher mobility than the main receptor band (Figure 2A, lane 0). A time course deglycosylation with PNGase F, followed by SDS–PAGE and immunoblotting, showed that both bands collapsed into a new band with higher mobility, suggesting that the bands correspond to di-, mono- and deglycosylated species, from top to bottom (Fig. 2A). The relative intensity of the bands before PNGase F treatment indicated that one site was glycosylated in ~75% of the species (site 1), and the second site in nearly 100% (site 2). Site 1 was easily accessible to PNGase F, as deglycosylation was complete in a few seconds, whereas glycan removal from site 2 was slow even at room temperature.

By comparison, 5–HT_4R expressed in mouse rod cells was glycosylated more homogeneously than 5–HT_4R expressed in the mammalian cell lines, HEK293 and TRex, but similarly to the receptor expressed in Sf9 cells, as assessed by electrophoresis (Figure S2). We did not determine which 5–HT_4R residues are glycosylated in insect cells but, because deglycosylation proceeded relatively rapidly and quantitatively, we speculate that only site 1 is glycosylated.

To confirm the electrophoretic results obtained for 5–HT_4R expressed in mouse rod cells, we carried out a detailed MS analysis of 5–HT_4R purified by sequential T7 and 1D4 immunochromatography. The purified receptor was separated by SDS–PAGE to allow independent analysis of monomers and dimers because, as with other GPCRs, receptor oligomerization is often visible in electrophoresis gels. Monomer and dimer bands were cut out and treated separately with in–gel trypsin or chymotrypsin digestion, but both bands produced identical results. Overall peptide coverage for 5–HT_4R in this study was 85% (Figure S3). The glycosylation site N^7 was identified by a mass increase of 0.9846 Da resulting from transformation of an Asn to an Asp residue after PNGase F treatment (Figure 2B and Figure 3), as well as by comparing the LC/MS profiles of glycosylated and deglycosylated 5–HT_4R peptides at the same elution time. As shown in Figure 3, the N^7 containing peptide ^{4}LDANVSSEEGFGSVEK^{19} (m/z of 834.40(2+)) and its glycoforms were observed within an elution time period of 4 min. After PNGase F treatment, the heterogeneous glycopeptide peaks disappeared and a new 834,89(2+) peak was formed corresponding to the peptide with N^7 converted to a D residue by PNGase F. Because the free peptide with m/z of 834.40(2+) was also observed in the PNGase F-treated sample, glycan modification at the N^7 residue was not 100%. Further quantitative glycosylation mapping was carried out by calculating the ratios of selected ion chromatogram peak areas of converted N/D peptide to total converted and un–converted peptides. It should be noted that deamidation of an Asn residue resulting from loss of ammonia and formation of an Asp residue causes the exact same mass increase of +0.9846. Thus, the ratio resulting from deamidation *in vivo* and *in vitro* must be excluded, which can be estimated from the 5–HT_4R

sample not treated with PNGase F. The deamidation ratio of N^7 was found to be negligible (data not shown), and the glycan occupancy at N^7 was determined to be ~70% (Figure 2B). Identification of the glycosylation species present at N^{180} was challenging. Neither unmodified nor Asn/Asp converted glycan–free peptides were detected in either glycosylated or de–glycosylated 5–HT_4R, suggesting either a site fully occupied by glycans and/or poor ionization of the peptides. However, glycopeptides consistent with the chymotryptic peptide ^{176}NQNSNSTYCVF^{186} along with various glycan moieties at N^{180} were identified with a mass error of less than 5 ppm by glycopeptide mapping. The tandem mass spectrum of each glycopeptide further confirmed glycan compositions at the specific glycosylation sites (Figure S4). Therefore, the monoglycosylated form of the receptor observed in electrophoresis (Figure 2A) which was slowly deglycosylated by PNGase F corresponds to N^{180}, site 2 in E–II loop, whereas site 1 (easily accessible to PNGase F) corresponds to N^7 in the N-terminus.

The different glycosylation species identified for 5–HT_4R expressed in the retina of TG mice are summarized in Table 1. High mannose type and complex type of sugars were identified at both sites. Most of the oligosaccharides had the core structure of three mannose (Man) and two N–acetylglucosamine (GlcNAc) residues Manα1→3–(Manα1→6)Manβ1→4GlcNAcβ1→4GlcNAc→Asn (or $(Hex)_3(GlcNAc)_2$ in the abbreviated nomenclature used in Table 1) common in vertebrate N–glycosylated proteins. LC-MS/MS identified a total of 23 species for N^7, and 8 species for N^{180}, which explains the smearing of the upper band noted in the SDS–PAGE gels (Figure 2A).

The glycosylation pattern observed for 5–HT_4R was unexpectedly complex such that the receptor migrated as two distinct electrophoretic bands (Figure 4, lane 1). In contrast, four other GPCRs, also expressed in TG mouse rod cells (cannabinoid CB2 receptor, AA1AR, 5–HT_{2C}R and 5–HT_7R), migrated as single electrophoretic bands (Figure S5 and (11)). PNGase F treatment of these receptors showed that they were glycosylated (not shown), but we did not carry out a detailed glycan analysis.

It could be argued that heterogeneity of 5–HT_4R glycans as identified by mass spec is artifactually influenced by in–source fragmentation. Actually, this method has been used to detect glycopeptides by monitoring low–mass, sugar–specific oxonium ions (24, 25). However, in-source fragmentation must be specifically enabled. In our experiments, no active source fragmentation was applied. Therefore heterogeneity of glycans from in-source fragmentation here should be negligible.

To place the glycosylation heterogeneity of 5–HT_4R in TG mice in some perspective, we compared it to co-expressed rhodopsin from the same TG mice. Mouse rhodopsin was purified with immobilized 1D4 antibody from the flow–through remaining after purification of 5–HT_4R with immobilized T7 antibody. With this preparation, we then confirmed the presence of analogous glycosylation sites N^2 and N^{15} in mouse rhodopsin and identified the nature of their glycans (Table 1). Again, we were surprised by the large variety of distinct glycosyl species identified (7 for N^2 and 18 for N^{15}).

A possible cause for the heterogeneity of rhodopsin glycosylation in TG mice is that 5–HT_4R was being co–expressed with rhodopsin, thereby stressing the PTM machinery in rod cells. Thus, we also analyzed the glycosylation pattern of rhodopsin from WT mice. The results (Table 1) confirm this hypothesis, as the heterogeneity of rhodopsin glycosylation in WT mice was markedly reduced at N^{15}. Nevertheless, a number of distinct glycosylation species were observed by LC-MS/MS for rhodopsin from WT mice. Bovine rhodopsin is known for its homogeneous glycosylation pattern, which has allowed its crystallization in at least 5 different asymmetric unit arrangements without prior deglycosylation (26). For this

reason, we also included bovine rhodopsin in the glycan analysis (Table 1). Eight glycosyl species were found at the N^2 position and 10 at the N^{15} position in bovine rhodopsin. The predominant oligosaccharide form in bovine rhodopsin is: GlcNAcβ1→2Manα1→3–(Manα1→6)Manβ1→4GlcNAcβ1→4GlcNAc→Asn (or $(Hex)_1$+$(Man)_3(GlcNAc)_2$ in the nomenclature shown in Table 1). We found that this accounted for ~50% of the glyco species at N^{15} in bovine rhodopsin (not shown). This glyco form was previously reported to be the major oligosaccharide structure in bovine rhodopsin (27) and accounted for ~60% of the glyco forms in frog (28). This was also the major oligosaccharide we found at N^2, but its quantification was complicated because multiple ions were detected for the N^2-containing glycopeptide (due to incomplete N–terminal acetylation, oxidation of M^1 residue, and Na^+ complexes, etc.).

The relative heterogeneity of glycosylation found for the four proteins analyzed by LC-MS/MS (5–HT_4R and rhodopsin in TG mice, rhodopsin in WT mice and bovine rhodopsin) is consistent with the smeared appearance of electrophoretic bands observed before treatment with PNGase F (Figure 4).

Similar to 5–HT_4R, when we expressed rhodopsin in mammalian cell culture, a complex hyperglycosylation pattern was found by SDS-PAGE that precluded MS analysis of the individual glycosylated species (Figure S6).

Phosphorylation of 5–HT_4R

Although Ser, Thr and Tyr residues typically can be phosphorylated by a variety of cellular kinases, the only major kinase present in rod outer segments is the Ser/Thr protein kinase, GRK1, that specifically phosphorylates activated rhodopsin at three Ser residues in its C–terminus (29). *In vivo*, 5-HT4R can be phosphorylated by GRK5 at its C-terminal S/T (347–355) cluster (30). There are 19 potential phosphorylation targets for GRK1 in the intracellular region of 5–HT_4R: five Ser residues and one Thr in the C–III loop, plus six Ser residues and seven Thr residues in the C–terminus (including residues in the purification tags). Because initial experiments in which we treated purified 5–HT_4R with phosphatase PP2A suggested that this receptor was phosphorylated (Figure S7), we analyzed the phosphorylation status of heterologously expressed 5-HT_4R.

LC/MS indicated that a peptide corresponding to the third intracellular loop (A^{232} to R^{250}) evidenced highly heterogeneous phosphorylation (Figure 5 and Table 2). Tandem mass spectra of this peptide revealed the identity of the phosphorylated residues for each species through their cleavage precursors (both from the C–terminal and N–terminal directions) (Figure S8). We found that S^{235}, S^{236}, S^{238} and S^{242} residues were the targets for phosphorylation in this peptide. For residues S^{247}/T^{248} in the C–III loop, it was not possible to unambiguously identify which of the 2 residues was phosphorylated. For Figure 5, the peak area of each extracted ion was calculated. Although the ionization efficiency of phosphorylated and unphosphorylated peptides is different, comparison of the corresponding chromatography areas can provide us some approximate information about their relative abundance. For peptide ^{232}AGASSESRPQSADQHSTHR^{250}, the ratio of un-/mono-/di-/tri-/tetra-phosphorylated species was about 1:47:50:22:3.

Similarly, multiple products with zero to five phosphorylated residues were found for the tryptic peptide R^{336}–R^{359} at the C–terminus (Table 2). In this case though, only S^{338} was positively identified as being phosphorylated. There are eight possible phosphorylation targets close together in peptide R^{336}-R^{359}, making it difficult to unambiguously identify individual phosphorylated residues.

Palmitoylation of 5–HT_4R

The MASCOT search of LC-MS/MS data showed a tryptic peptide ^{322}AFLIILCCDDER^{333} with m/z of 853.47(2+) singly palmitoylated (with the other Cys residue carboxamidomethylated) at positions C^{328} or C^{329} (both predicted to be situated immediately after helix 8). The un-palmitoylated peptide with m/z of 762.87(2+) (both C^{328} and C^{329} were carboxamidomethylated) was detected around the elution time of 30 min. The addition of a 16-carbon fatty acid to Cys residues turned the peptide into a very hydrophobic molecule, delaying the elution time more than 25 min. As shown in Figure 6A, there were two separate peaks, 56.99 min and 57.77 min, corresponding to the palmitoylated ion of 853.47(2+), and the area ratio of the two peaks was about 1:5. Hence, it is clear that there were two populations of palmitoylated peptides; one palmitoylated at C^{328} and the other at the C^{329} residue. Further deconvolution of tandem mass spectrum of these two elution fractions (at 57.77 min and 56.99 min), confirmed the palmitoylation at C^{328} and C^{329} (Figure 6B and 6C), respectively. Fragment ions y_5 and b_7 (as well as y_5* and b_7*) were critical for this distinction as shown in Figure 6D. Therefore, the ratio of palmitoylation at C^{328} to C^{329} was about 5:1. A di-palmitoylated form of this peptide was not detected.

Two Cys residues in the peptide ^{97}TSLDVLLTTASIFHLCCISLDR^{118} were also found to be partially palmitoylated (not shown). Because these residues are located deep within transmembrane region on helix III, we believe these are chemical modifications which occurred during the treatment of the sample after purification. Alternatively, they could represent an aberrant palmitoylation of misfolded proteins.

DISCUSSION

PTMs are important for biosynthesis and processing, including folding and trafficking, of membrane proteins. Experimentally, highly heterogeneous PTMs can present a considerable barrier to structural elucidations by crystallographic methods because crystal growth requires identical points of interaction between proteins in the crystal lattice. Given that different expression systems (including native expression in different tissues) can produce different PTMs for any given protein, it is prudent to characterize the PTMs involved before embarking on costly structure/function studies. And, as shown in this work, tight SDS–PAGE bands widely used to assess homogeneity of a protein sample are poor indicators of PTM homogeneity.

Previously we reported development of a GPCR expression system in *Xenopus* and murine rod cells, and demonstrated that GPCRs can be expressed in a functional form with apparently low heterogeneity ((10), (11), (9) and this work). Here we present a more detailed MS analysis of 5–HT_4R expressed in mice and show that its glycosylation is in fact quite heterogeneous. In addition, glycans at $N^{180;5.26}$ (in the Ballesteros-Weinstein numbering (31)) proved refractory to PNGase F treatment, as revealed by electrophoresis combined with LC-MS/MS. An analogous residue in the E–II loop of the β_2-adrenergic receptor ($N^{187;5.26}$), which is mutated in all β_2 adrenergic receptor structures to date, has also been shown to be inaccessible to PNGase F (32). The distal portion of the β_2 adrenergic receptor E–II loop makes close contacts with the E–I loop (33) and polysaccharides at $N^{187;5.26}$ may mask a group of aromatic residues in the E–I loop (34). In contrast, $N^{154;4.75}$ located in the proximal portion of E–II loop of the adenosine receptor 2A E-II loop can easily be enzymatically deglycosylated (35).

Our results obtained from TG mice suggest that stresses exerted on the glycosylation machinery due to the overexpression of an exogenous GPCR in rod cells may be responsible for the observed increase in glycosylation heterogeneity of endogenous rhodopsin at N^{15}. It

can therefore be supposed that non–native glycosylation of native and recombinant proteins in heterologous expression systems is a common occurrence.

In any case, bovine rhodopsin was even more homogenously glycosylated than mouse rhodopsin. Eight glycosylation species were found for N^2 and ten for N^{15} in bovine rhodopsin, with $(Hex)_1+(Man)_3(GlcNAc)_2$ accounting for about 50% of the total. In our crystal structure of photoactivated bovine rhodopsin (PDB ID 2I37), we were able to partially model the oligosaccharides at both N^2 and N^{15} despite the limited resolution (36). In monomer B, we modeled the linear pentasaccharide GlcNAc–Man–Man–GlcNAc–GlcNAc–N^{15}. Oligosaccharides at both N^2 and N^{15} are wrapped around the equivalent glycan from another monomer in the same unit cell. In addition, the mentioned pentasaccharide at N^{15} from monomer B was found to interact head–to–head with the equivalent glycan of monomer B from another unit cell in a manner that could not accommodate a longer oligosaccharide (Figure 3 in (36)). With this observation in mind, the question immediately arises as to how can a heterogeneously glycosylated protein such as bovine rhodopsin form crystals wherein multiple intermolecular glycan–glycan contacts stabilize both the rhombohedral (R32) and trigonal ($P3_112$) crystal forms ((26, 36)). One possible answer could be that minor species incompatible with this arrangement due to steric hindrance are omitted from the crystal. Another speculation is that there is enough room in the solvent cavity of the crystal to allow some flexibility and heterogeneity for branched glycans at N^{15} (Figure 3 in (36) and Figure 1 in (26)). (The rhombohedral cell contains ~80% solvent whereas the trigonal crystal form contains ~71% solvent). Therefore it seems that complete glycan homogeneity can be helpful but not always absolutely required for protein crystallization, even when these moieties appear favorably positioned to support intermolecular interactions present in some crystal lattices. However, the fact that mouse rhodopsin is glycosylated slightly more heterogeneously than bovine rhodopsin could have made its crystallization more difficult.

We also confirmed that 5–HT_4R heterologously expressed in TG mouse retina was phosphorylated, conforming with reports that activated rhodopsin can enhance GRK1-mediated phosphorylation of exogenous proteins in the retina (37). However, the level and heterogeneity of 5-HT_4R phosphorylation was unexpected because GRK1 (the only GRK present in rod outer segments) only phosphorylates three Ser residues in the C–terminus of rhodopsin in a light–dependent manner (29) despite the abundance of Ser and Thr residues in rhodopsin's C–terminus and C–III loop. Consequently, we then routinely treated 5–HT_4R with mouse protein phosphorylase PP2A during its purification, to eliminate or minimize the number of phosphorylated residues. MS results also indicate that 5–HT_4R is heterogeneously phosphorylated in the C–III loop and C–terminus when overexpressed in Sf9 insect cells (unpublished results).

The function of GPCR palmitoylation, or at least the need for palmitoylation for proper folding and function in some GPCRs, is still controversial. Recently we found that removal of palmitoylation in rhodopsin produced minor but cumulative effects resulting in defective vision, mainly because of palmitoylation's stabilizing effect on the unliganded receptor (opsin) (38). On the other hand, palmitoyl chains have markedly different conformations in the various rhodopsin crystal structures determined to date, and the β1 adrenergic receptor has been crystallized with the C358A mutation, removing the palmitoylation site altogether (39). These recent results suggest that palmitoylation is not essential for crystallization of naturally palmitoylated GPCRs, but we have yet to learn what the effect(s) of heterogeneous palmitoylation, as in the case of 5–HT_4R expressed in mouse rod cells, would be on GPCR crystallization.

In summary, we have shown that heterogeneity of PTMs in membrane proteins can easily be overlooked based on the SDS-PAGE and SEC metrics normally used to assess such constructs, potentially leading to negative effects on functional/structural studies. In the case of 5–HT_4R, glycosylation, phosphorylation and palmitoylation were heterogeneous with respect to both the identities and total numbers of modified residues. This encouraged us to make changes in the construct and/or purification protocol to eliminate, or at least minimize such heterogeneity prior to crystallization trials. Heterogeneity of glycosylation in rod cells appears to be receptor– (or receptor family–) dependent, because several GPCRs heterologously expressed in either *Xenopus* or mouse rod cells showed considerably less heterogeneity of glycosylation than 5–HT_4, 5–HT_{2A} and 5–HT_7 receptors, as judged by electrophoreric criteria (this work, (9) (11) and non–published data).

Supplementary Material

Refer to Web version on PubMed Central for supplementary material.

Acknowledgments

We thank Dr. Leslie T. Webster, Jr., David T. Lodowski and the Palczewski laboratory for critical comments on the manuscript.

References

1. Bockaert J, Claeysen S, Becamel C, Pinloche S, Dumuis A. G protein-coupled receptors: dominant players in cell-cell communication. Int Rev Cytol. 2002; 212:63–132. [PubMed: 11804040]
2. Nichols DE, Nichols CD. Serotonin receptors. Chem Rev. 2008; 108:1614–1641. [PubMed: 18476671]
3. Berger M, Gray JA, Roth BL. The expanded biology of serotonin. Annu Rev Med. 2009; 60:355–366. [PubMed: 19630576]
4. Bockaert J, Claeysen S, Compan V, Dumuis A. 5-HT(4) receptors, a place in the sun: act two. Curr Opin Pharmacol. 2011; 11:87–93. [PubMed: 21342787]
5. Aitken, A. Protein chemistry methods posttranslational modification, consensus sequences. In: Price, NC., editor. Proteins Labfax. Bios Scientific Publishers, Oxford; Academic Press, San Diego; San Diego: 1995. p. 253-285.
6. Witze ES, Old WM, Resing KA, Ahn NG. Mapping protein post-translational modifications with mass spectrometry. Nat Methods. 2007; 4:798–806. [PubMed: 17901869]
7. Deribe YL, Pawson T, Dikic I. Post-translational modifications in signal integration. Nat Struct Mol Biol. 2010; 17:666–672. [PubMed: 20495563]
8. Skropeta D. The effect of individual N-glycans on enzyme activity. Bioorg Med Chem. 2009; 17:2645–2653. [PubMed: 19285412]
9. Zhang L, Salom D, He J, Okun A, Ballesteros J, Palczewski K, Li N. Expression of functional G protein-coupled receptors in photoreceptors of transgenic Xenopus laevis. Biochemistry (Mosc). 2005; 44:14509–14518.
10. Salom D, Wu N, Sun W, Dong Z, Palczewski K, Jordan S, Salon JA. Heterologous expression and purification of the serotonin type 4 receptor from transgenic mouse retina. Biochemistry (Mosc). 2008; 47:13296–13307.
11. Li N, Salom D, Zhang L, Harris T, Ballesteros JA, Golczak M, Jastrzebska B, Palczewski K, Kurahara C, Juan T, Jordan S, Salon JA. Heterologous expression of the adenosine A1 receptor in transgenic mouse retina. Biochemistry (Mosc). 2007; 46:8350–8359.
12. MacKenzie D, Arendt A, Hargrave P, McDowell JH, Molday RS. Localization of binding sites for carboxyl terminal specific anti-rhodopsin monoclonal antibodies using synthetic peptides. Biochemistry (Mosc). 1984; 23:6544–6549.
13. Papermaster DS. Preparation of retinal rod outer segments. Methods Enzymol. 1982; 81:48–52. [PubMed: 6212746]

14. Salom D, Le Trong I, Pohl E, Ballesteros JA, Stenkamp RE, Palczewski K, Lodowski DT. Improvements in G protein-coupled receptor purification yield light stable rhodopsin crystals. J Struct Biol. 2006; 156:497–504. [PubMed: 16837211]
15. Ikehara T, Shinjo F, Ikehara S, Imamura S, Yasumoto T. Baculovirus expression purification, and characterization of human protein phosphatase 2A catalytic subunits alpha and beta. Protein Expr Purif. 2006; 45:150–156. [PubMed: 16039140]
16. Tsybovsky Y, Wang B, Quazi F, Molday RS, Palczewski K. Posttranslational Modifications of the Photoreceptor-Specific ABC Transporter ABCA4. Biochemistry. 2011; 50:6855–6866. [PubMed: 21721517]
17. Reeves PJ, Thurmond RL, Khorana HG. Structure and function in rhodopsin: high level expression of a synthetic bovine opsin gene and its mutants in stable mammalian cell lines. Proc Natl Acad Sci U S A. 1996; 93:11487–11492. [PubMed: 8876162]
18. Mollaaghababa R, Davidson FF, Kaiser C, Khorana HG. Structure and function in rhodopsin: expression of functional mammalian opsin in Saccharomyces cerevisiae. Proc Natl Acad Sci U S A. 1996; 93:11482–11486. [PubMed: 8876161]
19. Salom, D.; Palczewski, K. Production of Membrane Proteins. Wiley-VCH Verlag GmbH & Co. KGaA; 2011. Structural Biology of Membrane Proteins; p. 249-273.
20. Claeysen S, Sebben M, Journot L, Bockaert J, Dumuis A. Cloning expression and pharmacology of the mouse 5-HT(4L) receptor. FEBS Lett. 1996; 398:19–25. [PubMed: 8946946]
21. Beck-Sickinger AG. Structural characterization and binding sites of G-protein-coupled receptors. Drug Disc Today. 1996; 1:502–513.
22. Baneres JL, Mesnier D, Martin A, Joubert L, Dumuis A, Bockaert J. Molecular characterization of a purified 5-HT4 receptor: a structural basis for drug efficacy. J Biol Chem. 2005; 280:20253–20260. [PubMed: 15774473]
23. Fredericks ZL, Pitcher JA, Lefkowitz RJ. Identification of the G protein-coupled receptor kinase phosphorylation sites in the human beta2-adrenergic receptor. J Biol Chem. 1996; 271:13796–13803. [PubMed: 8662852]
24. Hirohata S, Wang LW, Miyagi M, Yan L, Seldin MF, Keene DR, Crabb JW, Apte SS. Punctin a novel ADAMTS-like molecule, ADAMTSL-1, in extracellular matrix. J Biol Chem. 2002; 277:12182–12189. [PubMed: 11805097]
25. Mechref Y, Madera M, Novotny MV. Assigning glycosylation sites and microheterogeneities in glycoproteins by liquid chromatography/tandem mass spectrometry. Methods Mol Biol. 2009; 492:161–180. [PubMed: 19241032]
26. Lodowski DT, Salom D, Le Trong I, Teller DC, Ballesteros JA, Palczewski K, Stenkamp RE. Crystal packing analysis of Rhodopsin crystals. J Struct Biol. 2007; 158:455–462. [PubMed: 17374491]
27. Fukuda MN, Papermaster DS, Hargrave PA. Rhodopsin carbohydrate. Structure of small oligosaccharides attached at two sites near the NH2 terminus. J Biol Chem. 1979; 254:8201–8207. [PubMed: 468821]
28. Duffin KL, Lange GW, Welply JK, Florman R, O'Brien PJ, Dell A, Reason AJ, Morris HR, Fliesler SJ. Identification and oligosaccharide structure analysis of rhodopsin glycoforms containing galactose and sialic acid. Glycobiology. 1993; 3:365–380. [PubMed: 8400551]
29. Ohguro H, Palczewski K, Ericsson LH, Walsh KA, Johnson RS. Sequential phosphorylation of rhodopsin at multiple sites. Biochemistry (Mosc). 1993; 32:5718–5724.
30. Barthet G, Carrat G, Cassier E, Barker B, Gaven F, Pillot M, Framery B, Pellissier LP, Augier J, Kang DS, Claeysen S, Reiter E, Baneres JL, Benovic JL, Marin P, Bockaert J, Dumuis A. Beta-arrestin1 phosphorylation by GRK5 regulates G protein-independent 5-HT4 receptor signalling. EMBO J. 2009; 28:2706–2718. [PubMed: 19661922]
31. Ballesteros JA, W H. Integrated methods for the construction of three dimensional models and computational probing of structure function relations in G protein-coupled receptors. Methods Neurosci. 1995; 25:366–428.
32. Rasmussen SG, Devree BT, Zou Y, Kruse AC, Chung KY, Kobilka TS, Thian FS, Chae PS, Pardon E, Calinski D, Mathiesen JM, Shah ST, Lyons JA, Caffrey M, Gellman SH, Steyaert J,

Skiniotis G, Weis WI, Sunahara RK, Kobilka BK. Crystal structure of the beta(2) adrenergic receptor-Gs protein complex. Nature. 2011

33. Mialet-Perez J, Green SA, Miller WE, Liggett SB. A primate-dominant third glycosylation site of the beta2-adrenergic receptor routes receptors to degradation during agonist regulation. J Biol Chem. 2004; 279:38603–38607. [PubMed: 15247302]
34. Cherezov V, Rosenbaum DM, Hanson MA, Rasmussen SG, Thian FS, Kobilka TS, Choi HJ, Kuhn P, Weis WI, Kobilka BK, Stevens RC. High-resolution crystal structure of an engineered human beta2-adrenergic G protein-coupled receptor. Science. 2007; 318:1258–1265. [PubMed: 17962520]
35. Jaakola VP, Griffith MT, Hanson MA, Cherezov V, Chien EY, Lane JR, Ijzerman AP, Stevens RC. The 2.6 angstrom crystal structure of a human A2A adenosine receptor bound to an antagonist. Science. 2008; 322:1211–1217. [PubMed: 18832607]
36. Salom D, Lodowski DT, Stenkamp RE, Le Trong I, Golczak M, Jastrzebska B, Harris T, Ballesteros JA, Palczewski K. Crystal structure of a photoactivated deprotonated intermediate of rhodopsin. Proc Natl Acad Sci U S A. 2006; 103:16123–16128. [PubMed: 17060607]
37. Palczewski K, Buczylko J, Kaplan MW, Polans AS, Crabb JW. Mechanism of rhodopsin kinase activation. J Biol Chem. 1991; 266:12949–12955. [PubMed: 2071581]
38. Maeda A, Okano K, Park PS, Lem J, Crouch RK, Maeda T, Palczewski K. Palmitoylation stabilizes unliganded rod opsin. Proc Natl Acad Sci U S A. 2010; 107:8428–8433. [PubMed: 20404157]
39. Warne T, Serrano-Vega MJ, Baker JG, Moukhametzianov R, Edwards PC, Henderson R, Leslie AG, Tate CG, Schertler GF. Structure of a beta1-adrenergic G-protein-coupled receptor. Nature. 2008; 454:486–491. [PubMed: 18594507]

ABBREVIATIONS

5–HT$_4$R	serotonin receptor type 4
AA1R	adenosine subtype A1 receptor
DDM	*n*–dodecyl–β–D–maltoside
GlcNAc	n–acetylglucosamine
GPCR	G–protein coupled receptor
LC	liquid chromatography
Man	mannose
MS	mass spectroscopy
PTM	post–translational modification
ROS	rod outer segment(s)
SEC	size-exclusion chromatography
TG	transgenic

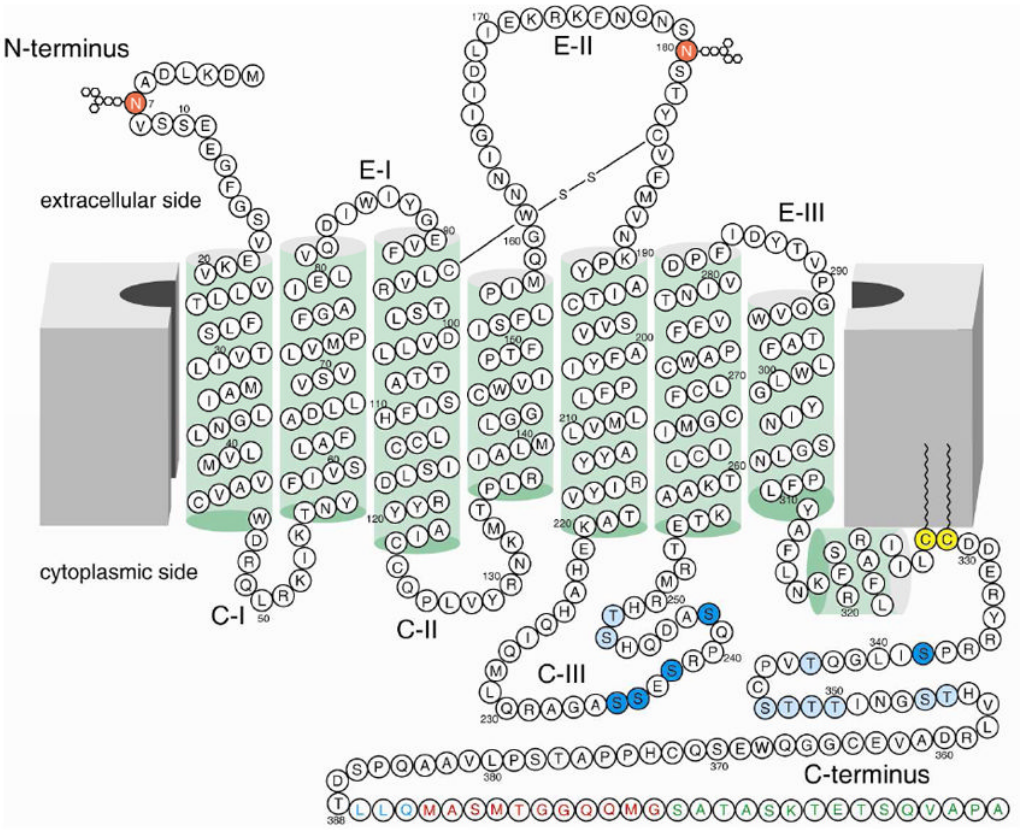

Figure 1.

Two–dimensional model of the 5–HT_{4b}R construct used in this work (based on the β1 adrenergic receptor structure, PDB ID 2VT4). Colored circles denote different PTMs found: red for glycosylation, blue for phosphorylation and yellow for palmitoylation. Light blue circles represent putatively modified residues. A disulfide bridge is predicted based on homology to other GPCRs and experimental evidence. Colored letters indicate the C–terminal linker (blue) and purification tags (red for T7 and green for 1D4 tags).

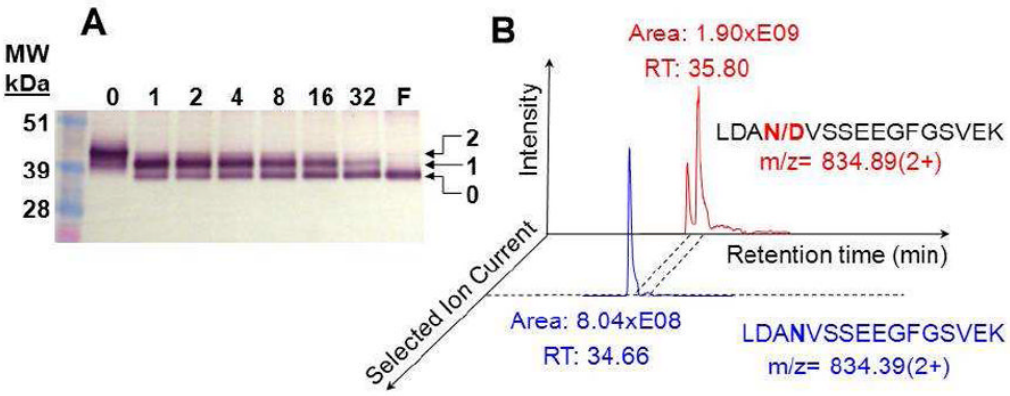

Figure 2.

Analysis of 5–HT_4R glycosylation. (A). Time course for PNGase F treatment of 5–HT_4R expressed in mouse rod cells. Numbers on top denote the time in minutes of incubation at room temperature of a DDM extract of transgenic mouse retina. At each time, an aliquot was taken and the deglycosylation reaction was stopped by adding electrophoresis loading buffer. The lane labeled F portrays the completed reaction, which was achieved by adding extra PNGase F to an aliquot and incubating the mixture for 1 h at 37°C. Arrows indicate the three major bands visible in the 1D4 immunoblot of a SDS–PAGE gel, corresponding to diglycosylated, monoglycosylated and deglycosylated protein, from top to bottom. The monoglycosylated form corresponds to receptor glycosylated at N^{180} (see text). (B). Extracted ion chromatogram of ^{4}LDANVSSEEGFGSVEK^{19} with m/z=834.39 (2+) and 834.89 (2+). N^{7} was converted to an Asp residue in PNGase F–treated 5–HT_4R.

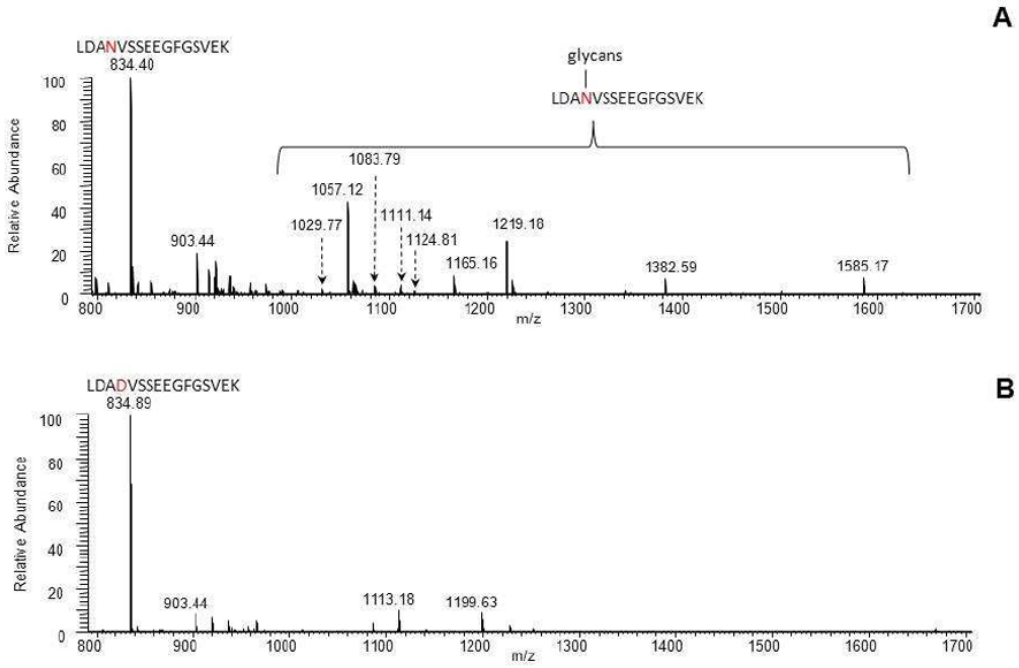

Figure 3.

Analysis of 5–HT_4R glycosylation. Mass spectral analysis of chromatographed peptide ^{4}LDANVSSEEGFGSVEK^{19} samples with m/z of 834.40 (2+) eluting at 32–36 min. (A). With different glycans; (B). Deglycosylated with PNGase F. Peak at 834.89 (2+) corresponds to the deglycosylated peptide with a mass shift of +0.980 Da emanating from conversion of the N^7 to a D^7 residue after PNGase F treatment.

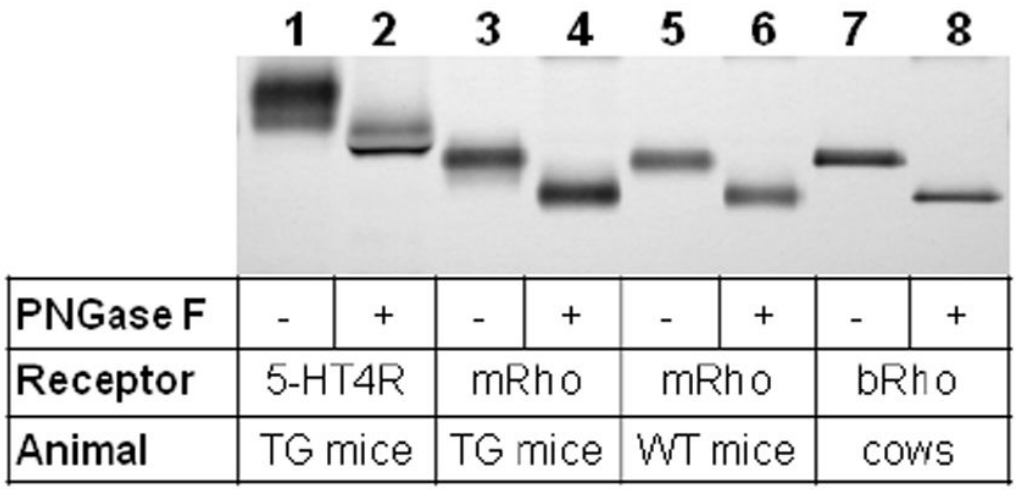

Figure 4.

1D4 immunoblots of purified receptors analyzed in this study, without and with PNGase F treatment. Lanes 1–2: 5–HT_4R. Lanes 3–4: Rhodopsin purified from 5–HT_4R transgenic mice. Lanes 5–6: Rhodopsin purified from WT mice. Lanes 7–8: Purified bovine rhodopsin. Smearing of the glycosylated protein bands parallels the heterogeneity of the glycosylation found by LC–MS/MS (see Table 1). 5–HT_4R (lane 2) was not completely deglycosylated; the monoglycosylated band is visible above the deglycosylated band.

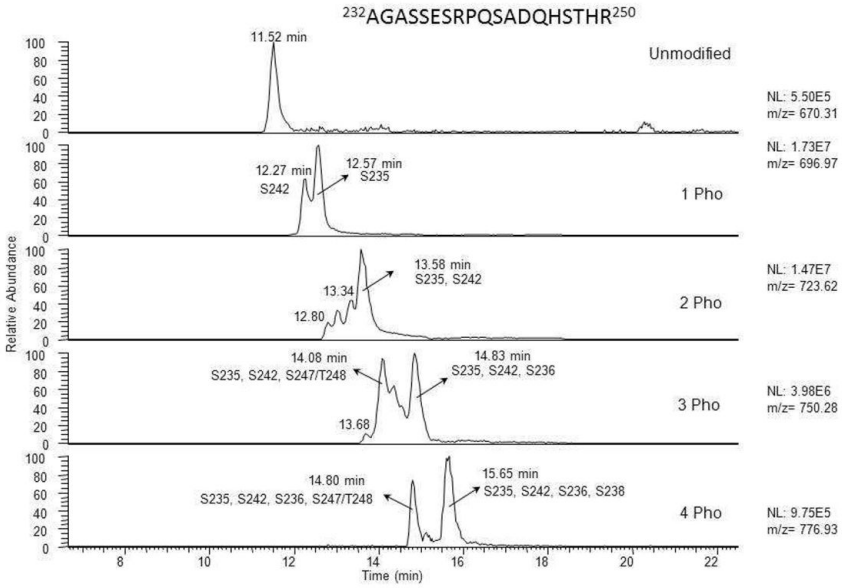

Figure 5.

Analysis of 5–HT_4R phosphorylation. Extracted ion chromatography of loop C–III peptide ^{232}AGASSESRPQSADQHSTHR^{250} with 0, 1, 2, 3 and 4 phosphorylated residues, respectively. NL stands for normalized peak intensity.

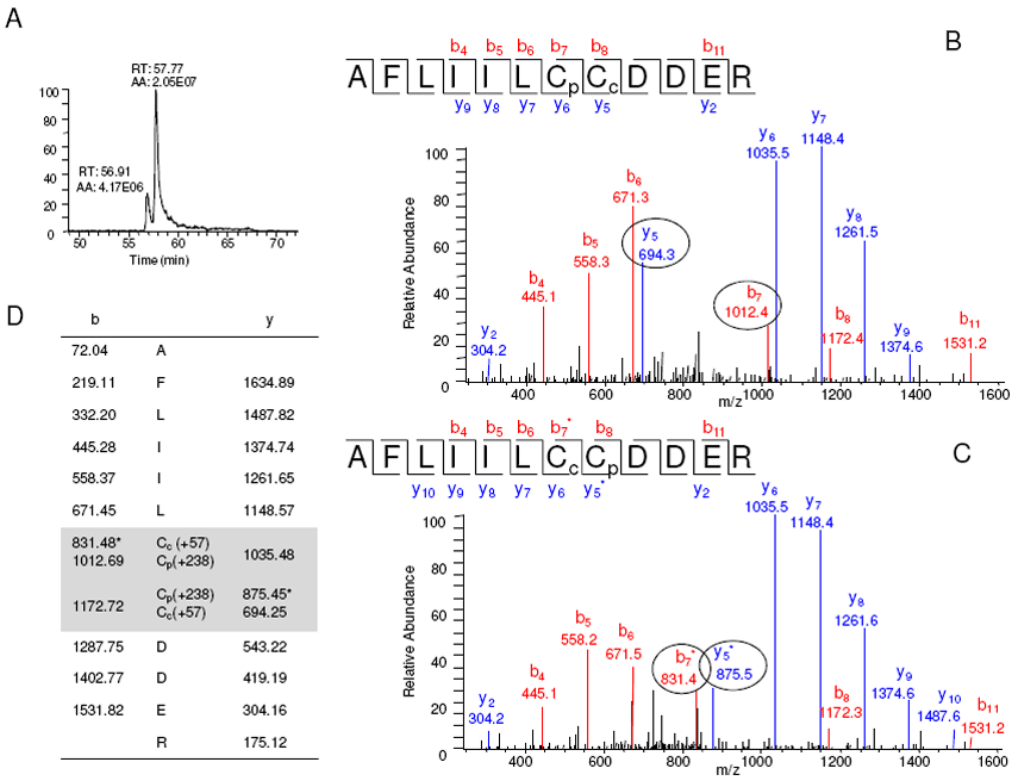

b		y
72.04	A	
219.11	F	1634.89
332.20	L	1487.82
445.28	I	1374.74
558.37	I	1261.65
671.45	L	1148.57
831.48* 1012.69	C_c (+57) C_p(+238)	1035.48
1172.72	C_p(+238) C_c(+57)	875.45* 694.25
1287.75	D	543.22
1402.77	D	419.19
1531.82	E	304.16
	R	175.12

Figure 6.

Analysis of 5–HT_4R palmitoylation. (A) Extracted ion chromatogram of the palmitoylated peptide ^{322}AFLIILCCDDER^{333} with m/z of 853.47 (2+). The mass shift of +295 compared with unmodified peptide corresponds to one Cys palmitoylated (C_p) and the other one carboxamidomethylated (C_c). Deconvoluted tandem mass spectrum of the peptide eluting at 57.77 min was assigned to C^{328} palmitoylation (B), and the 56.91 min elution to C^{329} palmitoylation (C). This is indicated by fragment ions of 694.3 (y_5), and 1012.4 (b_7) for C^{328} palmitoylation (B), as well as 875.5 (y_5*) and 831.4 (b_7*) for C^{329} palmitoylation (C). (D) Table listing the theoretical mass value of fragment ions corresponding the palmitoylation and carboxamidomethylation at C^{328} or C^{329}. Fragment ions in circle show the mass shift of 57.0215 (carboxamidomethylation, Cc) or 238.2297 (palmitoylation C_p). Parent ions are within 10 ppm for extracted ion chromatogram.

Table 1

Summary of 5–HT_4R and rhodopsin glycosylation in rod cells[a].

	Bovine rhodopsin	WT mouse rhodopsin	Mouse rhodopsin in $5HT_4$R TG mice		$5HT_4$R in TG mice
N^2	$(Hex)_2$ $(HexNAc)_2$	$(Hex)_2$ $(HexNAc)_2$	$(Hex)_2$+$(Man)_3(GlcNAc)_2$	**N^7**	$(Hex)_3(GlcNAc)_2$
	$(Hex)_3$ $(HexNAc)_2$	$(Hex)_3$ $(HexNAc)_2$	$(Hex)_3$+$(Man)_3(GlcNAc)_2$		$(HexNAc)_1$+$(Man)_3(GlcNAc)_2$
	$(Hex)_1$+$(Man)_3(GlcNAc)_2$	$(Hex)_1$ + $(Man)_3(GlcNAc)_2$	$(Hex)_4$+$(Man)_3(GlcNAc)_2$		$(Hex)_1(HexNAc)_1$+$(Man)_3(GlcNAc)_2$
	$(Hex)_2$+$(Man)_3(GlcNAc)_2$	$(Hex)_2$ + $(Man)_3(GlcNAc)_2$	$(Hex)_5$+$(Man)_3(GlcNAc)_2$		$(Hex)_2(HexNAc)_1$+$(Man)_3(GlcNAc)_2$
	$(HexNAc)_1$+$(Man)_3(GlcNAc)_2$	$(Hex)_3$ + $(Man)_3(GlcNAc)_2$	$(HexNAc)_1$+$(Man)_3(GlcNAc)_2$		$(Hex)_3(HexNAc)_1$+$(Man)_3(GlcNAc)_2$
	$(Hex)_1(HexNAc)_1$+$(Man)_3(GlcNAc)_2$	$(Hex)_4$ + $(Man)_3(GlcNAc)_2$	$(Hex)_1(HexNAc)_1$+$(Man)_3(GlcNAc)_2$		$(HexNAc)_2$+$(Man)_3(GlcNAc)_2$
	$(Hex)_2(HexNAc)_1$+$(Man)_3(GlcNAc)_2$	$(Hex)_5$ + $(Man)_3(GlcNAc)_2$	$(Hex)_2(HexNAc)_1$+$(Man)_3(GlcNAc)_2$		$(Hex)_1(HexNAc)_2$+$(Man)_3(GlcNAc)_2$
	$(Hex)_3(HexNAc)_1$+$(Man)_3(GlcNAc)_2$	$(HexNAc)_1$ + $(Man)_3(GlcNAc)_2$			$(Hex)_2(HexNAc)_2$+$(Man)_3(GlcNAc)_2$
		$(Hex)_1$ $(HexNAc)_1$ +$(Man)_3(GlcNAc)_2$			$(HexNAc)_3$+$(Man)_3(GlcNAc)_2$
		$(Hex)_2$ $(HexNAc)_1$ +$(Man)_3(GlcNAc)_2$			$(Hex)_1(HexNAc)_3$+$(Man)_3(GlcNAc)_2$
					$(Hex)_2(HexNAc)_3$+$(Man)_3(GlcNAc)_2$
N^{15}	$(Hex)_1$ $(HexNAc)_2$	$(Hex)_2$ $(HexNAc)_2$	$(Hex)_3(GlcNAc)_2$		$(Hex)_3(HexNAc)_3$+$(Man)_3(GlcNAc)_2$
	$(Hex)_2$ $(HexNAc)_2$	$(Hex)_3$ $(HexNAc)_2$	$(Hex)_1$+$(Man)_3(GlcNAc)_2$		$(HexNAc)_4$+$(Man)_3(GlcNAc)_2$
	$(Hex)_3$ $(HexNAc)_2$	$(Hex)_1$+$(Man)_3(GlcNAc)_2$	$(Hex)_2$+$(Man)_3(GlcNAc)_2$		$(Hex)_1(HexNAc)_4$+$(Man)_3(GlcNAc)_2$
	$(Hex)_1$+$(Man)_3(GlcNAc)_2$	$(Hex)_2$+$(Man)_3(GlcNAc)_2$	$(Hex)_3$+$(Man)_3(GlcNAc)_2$		$(Hex)_2(HexNAc)_4$+$(Man)_3(GlcNAc)_2$
	$(Hex)_2$+$(Man)_3(GlcNAc)_2$	$(HexNAc)_1$+$(Man)_3(GlcNAc)_2$	$(Hex)_4$+$(Man)_3(GlcNAc)_2$		$(Hex)_3(HexNAc)_4$+$(Man)_3(GlcNAc)_2$
	$(HexNAc)_1$+$(Man)_3(GlcNAc)_2$	$(Hex)_1(HexNAc)_1$+$(Man)_3(GlcNAc)_2$	$(Hex)_5$+$(Man)_3(GlcNAc)_2$		$(Hex)_4(HexNAc)_4$+$(Man)_3(GlcNAc)_2$
	$(Hex)_1(HexNAc)_1$+$(Man)_3(GlcNAc)_2$	$(Hex)_2(HexNAc)_1$+$(Man)_3(GlcNAc)_2$	$(Hex)_6$+$(Man)_3(GlcNAc)_2$		$(Hex)_1(HexNAc)_1(NeuAc)_1$+$(Man)_3(GlcNAc)_2$
	$(Hex)_2(HexNAc)_1$+$(Man)_3(GlcNAc)_2$	$(Hex)_3(HexNAc)_1$+$(Man)_3(GlcNAc)_2$	$(HexNAc)_1$+$(Man)_3(GlcNAc)_2$		$(Hex)_2(HexNAc)_1(NeuAc)_1$+$(Man)_3(GlcNAc)_2$
	$(Hex)_3(HexNAc)_1$+$(Man)_3(GlcNAc)_2$	$(HexNAc)_2$+$(Man)_3(GlcNAc)_2$	$(Hex)_1(HexNAc)_1$+$(Man)_3(GlcNAc)_2$		$(Hex)_3(HexNAc)_1(NeuAc)_1$+$(Man)_3(GlcNAc)_2$
	$(Hex)_3$ $(HexNAc)_1$ $(NeuAc)_1$ +$(Man)_3(GlcNAc)_2$	$(HexNAc)_3$+$(Man)_3(GlcNAc)_2$	$(Hex)_2(HexNAc)_1$+$(Man)_3(GlcNAc)_2$		$(Hex)_1(HexNAc)_3(NeuAc)_1$+$(Man)_3(GlcNAc)_2$
			$(Hex)_3(HexNAc)_1$+$(Man)_3(GlcNAc)_2$		$(Hex)_2(HexNAc)_3(NeuAc)_1$+$(Man)_3(GlcNAc)_2$
			$(HexNAc)_2$+$(Man)_3(GlcNAc)_2$		$(Hex)_3(HexNAc)_3(NeuAc)_1$+$(Man)_3(GlcNAc)_2$
			$(Hex)_1(HexNAc)_2$+$(Man)_3(GlcNAc)_2$		
			$(Hex)_2(HexNAc)_2$+$(Man)_3(GlcNAc)_2$	**N^{180}**	$(HexNAc)_1$+$(Man)_3(GlcNAc)_2$
			$(HexNAc)_3$+$(Man)_3(GlcNAc)_2$		$(Hex)_1(HexNAc)_1$+$(Man)_3(GlcNAc)_2$

Bovine rhodopsin	WT mouse rhodopsin	Mouse rhodopsin in $5HT_4R$ TG mice	$5HT_4R$ in TG mice
		$(Hex)_1(HexNAc)_3+(Man)_3(GlcNAc)_2$	$(Hex)_2(HexNAc)_1+(Man)_3(GlcNAc)_2$
		$(Hex)_2(HexNAc)_3+(Man)_3(GlcNAc)_2$	$(Hex)_3(HexNAc)_1+(Man)_3(GlcNAc)_2$
			$(HexNAc)_3+(Man)_3(GlcNAc)_2$
			$(Hex)_1(HexNAc)_3+(Man)_3(GlcNAc)_2$
			$(Hex)_2(HexNAc)_3+(Man)_3(GlcNAc)_2$

[a]Glycan compositions were identified by LC-MS/MS as described in Experimental Procedures. GlcNAc, n–acetylglucosamine; Hex, hexose; Man, mannose; HexNAc, N-acetylhexosamine; Man, mannose; NeuAc, N-acetylneuraminic acid.

The + sign indicates glycans added after the core structure of $(Man)_3(GlcNAc)_2$.

Table 2

Phosphorylation sites identified in 5–HT_4R from transgenic mice by LC-MS/MS[a].

Sequence	Mass difference	Phosphorylation sites
AGASSESRPQSADQHSTHR C-III loop	+ 1 phosphate	S^{235}, S^{242}
	+ 2 phosphates	S^{235} and S^{242}
	+ 3 phosphates	S^{235}, $S^{242}$and S^{236} S^{235}, S^{242} and S^{247} or T^{248}
	+ 4 phosphates	S^{235}, S^{242}, $S^{236}$and S^{238} S^{235}, S^{242}, S^{236} and S^{247} or T^{248}
RPSILGQTVPCSTTTINGSTHVLR C-terminus	+ 1 phosphate	S^{338}
	+ 2 phosphates	S^{338} and S^{354} or T^{355}
	+ 3 phosphates	S^{338} and other 2-4 residues among T^{243}, S^{247}, T^{248}, T^{249}, T^{250}, T^{251}, S^{354} and T^{355}
	+ 4 phosphates	
	+ 5 phosphates	

[a]This analysis was performed as described in Experimental Procedures.